Journal of Thermal Science Vol.17, No.2 (2008) 134−140

DOI: 10.1007/s11630-008-0134-6 **Article ID: 1003-2169(2008)02-0134-07**

Shock Wave Observation in Narrow Tubes for a Parametric Study on Micro Wave Rotor Design

Koji Okamoto[1] and Mikiya Araki[2]

1. Department of Aeronautics and Astronautics, University of Tokyo, 7-3-1, Hongo, Bunkyo-ku Tokyo 113-8656, Japan
2. Department of Mechanical Engineering, Gunma University, 1-5-1 Tenjin-cho, Kiryu, Gunma 376-8515, Japan

Wave rotor is expected to improve the performance of micro gas turbines drastically. In the wave rotor design, the rotor speed is determined principally by the tube length. Therefore, a longer tube is preferable for miniaturized wave rotors to avoid the difficulty in bearings and lubrication system, while it may yield thicker wall boundary layer, shock wave dissipation and so on. In the present study, an experimental apparatus was built to visualize the wave rotor internal flow dynamics in a narrow tube by schlieren method and Laser Doppler Anemometry. In addition, different lengths of the tube were adopted and compared to investigate the effect of wall friction. Finally, 2D numerical simulation was performed and the results were compared with those of experiments.

Keywords: wave rotor, shock wave, unsteady flow, micro propulsion, flow visualization.

Introduction

Recently, the research on micro and further miniaturized gas turbines is becoming vigorous for distributed electric generators, propulsion system for small air vehicles, mobile power source and so on[1−2]. However, there are several issues in such small gas turbines, e.g. high rotor speed, larger heat and viscous losses, and a wave rotor is expected to improve the gas turbine performance drastically[3]. A wave rotor consists of ducts (ports) and a rotor with many straight passages (cells). Each port charges or discharges the fresh air or combustion gas respectively, and shock and expansion waves are generated and propagate in the cells by the pressure difference between the ports.

Figure 1 shows the wave diagram of the four- port through-flow wave rotor[4], which is one of the promising candidates for gas turbine cycle. In this figure, the cells are moving downward and the pressure wave propagation is drawn with characteristic lines. As seen in this figure, the air compression process in the wave rotor depends on two shock waves, i.e. primary and reflected shock waves.

In the wave rotor design, the rotor speed is determined principally by the cell length. Therefore, a longer cell is preferable for ultra micro wave rotors in terms of the bearings and lubrication system, although it may imply thicker wall boundary layer, shock wave dissipation, interaction between shock waves and boundary layers and so on. Therefore, it is important to investigate the effect of wall friction on the shock wave propagation process in small and long cells.

In the present study, an experimental apparatus was built to visualize the internal flow dynamics of small tubes, in which the fundamental wave rotor flow dynamics was generated. Then, two test sections of different lengths were adopted to investigate the wall friction effect. Moreover, 2D numerical simulation was performed and the results were compared with the experimental ones.

Received: November 2007
Koji OKAMOTO: Assistant Professor

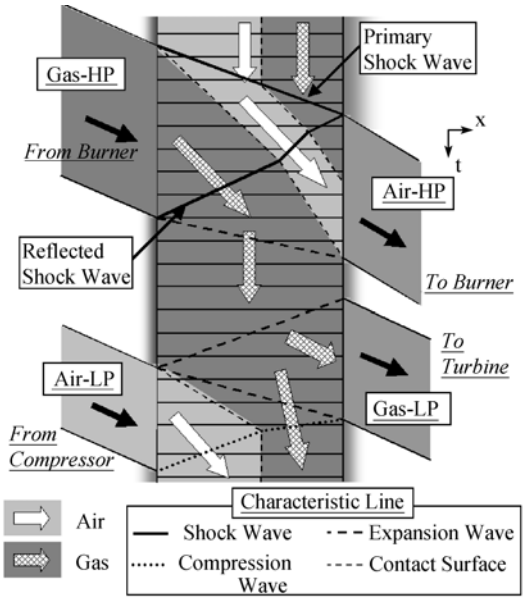

Fig.1 Wave Diagram

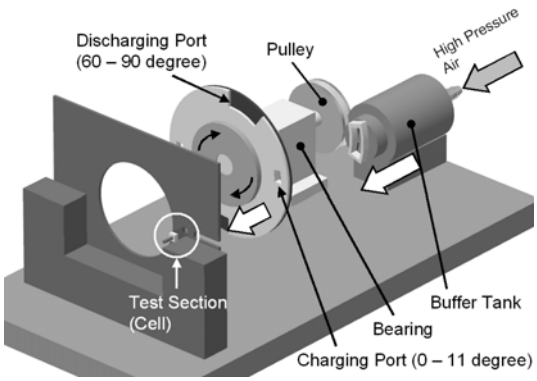

Fig.2 Experimental Apparatus for Visualization

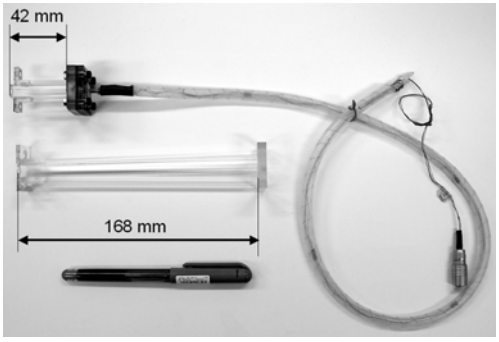

Fig. 3 Test Sections

Experiment and Numerical Analysis

Experimental Apparatus

Figure 2 shows the experimental apparatus used in this study. In this apparatus, the charging and discharging ports are rotating and a cell is fixed for easy measurement and visualization. This arrangement is completely opposite to the real wave rotors and the effect of rotation such as centrifugal force was not taken into consideration. However, the rotation effect does not have large influence on the pressure waves, according to the 3D numerical simulation[5]. In addition, only the charging and discharging ports are rotating at one end of the cell and another end is always closed. This configuration was introduced for simplicity and the fundamental flow dynamics is not much different from the real one.

In this experiment, high pressure air compressed by a screw compressor was provided as the driver gas, which was kept at 0.25 MPa and room temperature. First, the high pressure air is charged in the buffer tank, and then flows into the cell through the charging port and shock waves are generated. After that, the high pressure gas in the cell flows out to the surroundings in the radial direction through the discharging port. The rotor has two pairs of charging and discharging ports so that one rotation corresponds to two cycles.

In this experiment, two test sections of different lengths (42 mm and 168 mm) were prepared for comparison (Fig.3). The cross section is 3 mm square in both cases, and they are made of crystal glass. The right end is always closed with a pressure transducer, so that the high pressure air flows in and out from the left end. (In Fig.3, the pressure transducer is mounted on the short test section.)

As for the measurement, shock wave visualization with schlieren method, velocity measurement with Laser Doppler Anemometry (LDA) and stagnation pressure measurement were carried out. In the stagnation pressure measurement, a pressure transducer was mounted directly at the cell end, and the whole data acquisition system assures the frequency up to 100 kHz. For the shock wave visualization, a high speed CCD camera was adopted. The shutter speed was set to 500 ns and the timing of taking a photograph was controlled by the trigger pulse from the rotor. As for the LDA measurement, the flow velocity in the axial direction was measured. The system was set to measure the flow velocity in the range of –221 m/s and +368 m/s in each direction, and the size of measurement volume was 0.6 X 0.03 mm, approximately (Fig.4). The details of this LDA measurement were described in the reference[6].

Numerical Approach

2D numerical simulation was carried out at the mean rotor radius plane. The governing equations were two-dimensional Navier-Stokes equations considering laminar viscosity. The solution scheme was based on

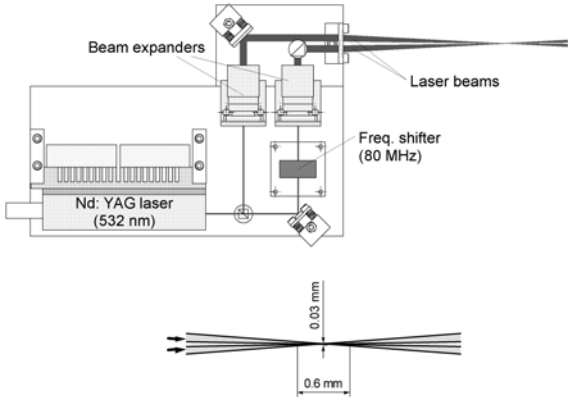

Fig.4 Schematics of the LDA Transmitter and Laser Beam Intersection Volume[6]

the finite difference method of discretization by incorporating Chakravarthy-Osher's third-order upwind TVD scheme with van Leer's differentiable limiter[7-8]. Jameson-Baker's four-stage Runge-Kutta scheme (fourth-order accuracy) was employed for time integration[9]. Time step was determined at every step by the maximum CFL number that was set to 1.0.

In the numerical simulation of wave rotors, the inflow and outflow boundary condition must be treated carefully, because the flow direction or flow velocity (supersonic or subsonic) is not known before each time step. In the present simulation, Riemann problem was solved between the conditions in the port and each boundary mesh to obtain the appropriate boundary condition at each time step[10]. On the other hand, ports' gradual opening and closing to the cell were simulated by gradually replacing the wall condition by the corresponding port condition.

The conditions in the ports were set as the same of the experiment and it was assumed to be uniform and constant, and the flow direction at the boundary was assumed to be axial during the simulation. As for the wall boundary condition, non-slip and adiabatic conditions were applied for all wall condition.

As for the calculation region, only the simulation of short test section (L=42mm) was performed in the present study. The cell region was discretized by 601 X 201 orthogonal grids. The leakage between the cell end and rotating ports was considered by adding the clearance region at the cell end. In the present simulation, the clearance gap was set as 0.4 mm, and the leakage flow in both the radial and circumferential direction was taken into consideration by estimating the flux at the boundary in each direction with Riemann solver[11].

Design Comparison

To compare the present designs with other wave rotors, three non-dimensional design parameters are introduced as follows.

Gradual Passage Opening:

$$\tau \equiv \left(Passage\,Opening\,Time\right)\Big/\left(Wave\,Travel\,Time\right) = \left(\frac{W_{cell}}{r\cdot\omega}\right)\Big/\left(\frac{L}{a}\right)$$

Wall Friction: $F = L/D_h$

Leakage: $G = 2\delta/H_{cell}$

Here, W_{cell} is the cell width; r, the mean rotor radius; ω, the angular speed of the rotor; a, the speed of sound; L, the cell length; D_h, the hydraulic diameter of the cell; δ, the axial clearance gap between the fixed end wall and the rotor and H_{cell}, the cell height. These three are the dominant performance loss factors, according to the previous experimental works[12-13], and the value of each parameter shows the amplitude of each performance loss.

Table 1 shows the comparison of these parameters with other wave rotors[4, 12-14]. As shown here, the present apparatus covers wide range of τ parameter value by changing the rotor speed (Table 2). As for F parameter,

Table 1 Design Comparison

	NASA (3-port)[13]	NASA & Allison[4]	Kentfield[13]	G.E.[12]	Comprex® (ABB)[14]	Visualization Test Rig (This work)
Length, L [m]	0.23, 0.46	0.152	0.28	0.3	0.0932	0.042, 0.168
Mean Radius, r [m]	0.15	0.0815	0.102	0.058	0.048	0.06
Cell Width, W_{cell} [m]	0.00635, 0.0127	0.00875	0.0168	0.01*	0.009	0.003
Cell Height, H_{cell} [m]	0.0102	0.022	0.0559	0.0231	0.01	0.003
Clearance, δ [mm]	0.127–0.381	0.13	0.18	0.64	0.15	0.4
Rotor Speed [rpm]	1850–7400	16800	5500	19000	14000	3600–10800
τ	0.08–0.35	0.194	0.35	0.0982**	0.467	0.18–1.1
$F = L/D_h$ ***	20–58	12.1	10.5	21.5	9.8	14, 56
$G = 2\,\delta/H_{cell}$	0.025–0.075	0.0118	0.006	0.0554	0.03	0.268

* Wall thickness between the cells included ** Calculated with atmospheric value *** D_h: Hydraulic Diameter

Table 2 Rotor Speed and τ Parameter Values for Operation

L = 42 mm			L = 168 mm		
Case	Rotor Speed [rpm]	τ	Case	Rotor Speed [rpm]	τ
S1	3600	1.10	L1	1800	0.55
S2	5400	0.73	L2	2700	0.37
S3	7200	0.55	L3	3600	0.27
S4	9000	0.44	L4	4500	0.22
S5	10800	0.37	L5	5400	0.18

the value of the short test section shows almost conventional, while that of the longer one shows almost maximum among these wave rotors. As easily found in the definition of these two parameters, longer cell allows slower rotor speed with keeping τ value, while it yields larger F value. Therefore, it is important to find a good balance of these two factors for the design of micro wave rotors. Also, the parameter value of leakage effect becomes large with size reduction, though this is not concerned with the present passage length difference.

Results

Shock Wave Visualization by Schlieren Method

Figure 5 shows the schlieren pictures of the case 'S3' in Table 2. In these pictures, 3 mm of the test section at the left end was not visualized due to fixing to the endwall. The time in this figure shows the time elapsed from the beginning of the charging port opening.

As seen in this figure, the primary shock wave begins to be observed at 60 μs. This is because the density gradient at the primary shock wave is not so steep at the beginning of the port opening by the gradual passage opening effect and then the pressure wave is gradually strengthened during the propagation. After that, the shock wave reflects around 90 μs at the right end and the reflected shock wave propagates to the left with almost constant speed. In this case, both of the shock waves can be observed clearly in the whole propagation process, once the primary shock wave becomes steep enough.

Figure 6 shows the schlieren pictures of the case "L3" in Table 2. As in the case of the short test section, the propagation process of these two shock waves can be observed clearly even in this case. Especially, it must be noticed that the reflected shock wave can be observed clearly without any obvious interaction with the wall boundary layer, even though it propagates against the inflow. Therefore, it can be concluded that the effect of boundary layer does not have large influence on the shock waves.

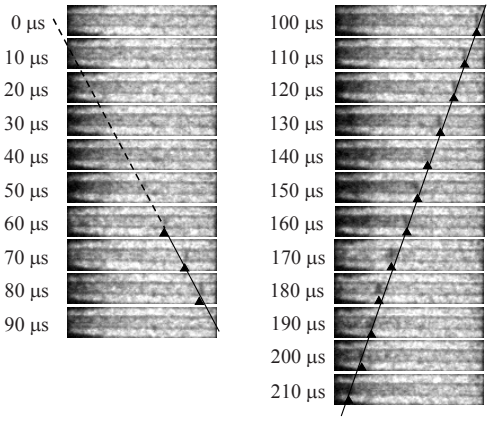

Fig.5 Schlieren Pictures (L=42 mm, 7200 rpm)

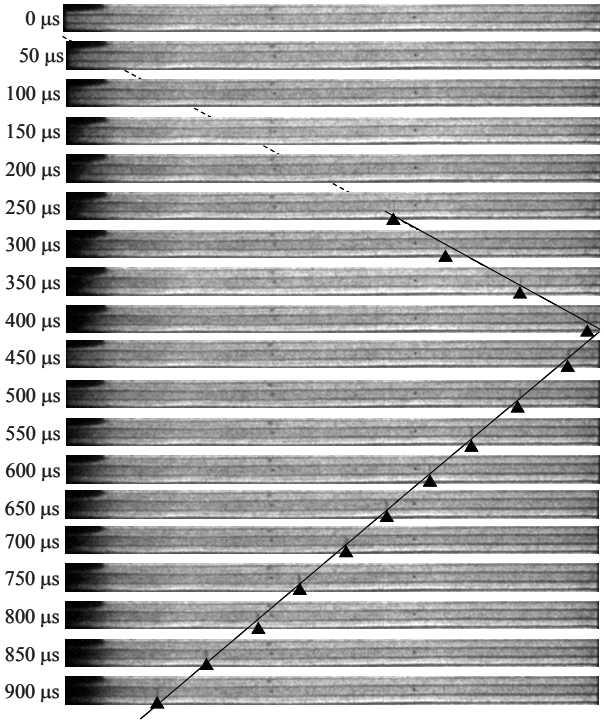

Fig.6 Schlieren Pictures (L=168 mm, 3600 rpm)

Velocity Measurement by LDA

Figure 7 shows the measuring points of each test section in the LDA measurement. The laser beams were set on the x-z surface in this figure, and the measurement was performed at 10 positions.

Figure 8 shows the result of the shorter cell (Case 'S3'), in which the abscissa axis indicates the rotation angle and 0 degree corresponds to the beginning of the charging port opening. First, the flow is accelerated suddenly by the primary shock wave arrival and the velocity reaches more than 200 m/s at x= 10 and 20 mm, even in this small cross section (3 mm square). Then, the flow is

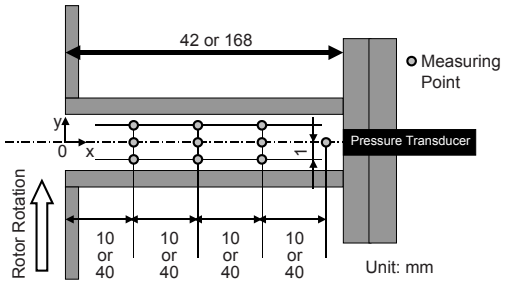

Fig.7 Measuring Points of LDA

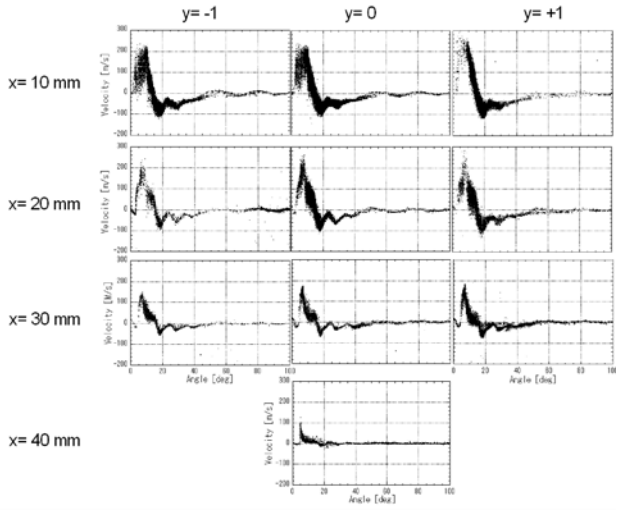

Fig.8 Velocity Distribution Measured by LDA (L=42 mm, 7200 rpm)

decelerated by the reflected shock wave, and the velocity becomes negative, even though either port is not opened to the cell during 14 and 60 degree rotor angle (the charging port starts closing at 11 degree and 3 mm cell width corresponds to about 3 degree). This is because the charged high pressure gas in the cell leaks to the outside through relatively large clearance gap. In addition, the particle density seems to decrease along the x direction, and its reason can be explained as follows: The particles mostly exist in the driver gas, and the flow velocity is much slower than the propagating velocity of the primary shock wave. Therefore, the driver gas with many particles is pushed back by the reflected shock wave before reaching the right end, and the density of the particles is not so high at the measuring points close to the stagnation.

Furthermore, it can be observed that the maximum velocity is not much different in the y direction at each x-position. Therefore, it can be concluded that the boundary layer thickness is less than 0.5 mm in this case, which seems to be consistent with the schlieren pictures.

Figure 9 shows the result of the longer cell (Case 'L3').

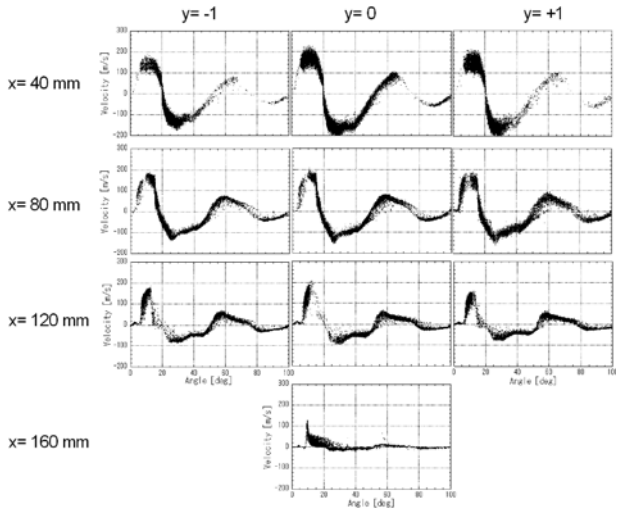

Fig.9 Velocity Distribution Measured by LDA (L=168 mm, 3600 rpm)

The basic flow dynamics is the same as in the shorter test section, even though some differences are appeared. The closing timing of charging port is 14 degree, while the arrival timing of reflected shock wave at x=40 mm is around 15 degree. (In the case of short test section, it is around 10 degree.) Therefore, the ports' rotation is too fast compared to the propagation of the reflected shock wave, which yields some qualitative difference.

As for the velocity distribution in y-direction, obvious difference of the peak velocity is not observed in either of the positive or negative directions at each x-position. Therefore, it can be concluded again that the boundary layer thickness is less than 0.5 mm, which seems to be small enough compared to the cross section size. This conclusion is consistent with the schlieren pictures, in which the reflected shock wave can be observed clearly without obvious interaction with the wall boundary layer.

Pressure Measurement at the Stagnation

Figure 10 shows the time traces of the stagnation pressure in the shorter test section of each rotor speed. When the rotor speed is 3600 and 5400 rpm, the increasing rate of pressure is much less than the other results. Meanwhile, when the rotor speed is faster than 7200 rpm, the increasing rate of pressure does not differ according to the faster rotor speed, even though the τ parameter value decreases. Also in the schlieren pictures, the propagating shock waves could not be observed when the rotor speed is slower than 5400 rpm, even though those schlieren pictures are not shown in this paper. Therefore, it can be concluded that the primary shock wave became a real shock wave during its propagation when the rotor speed is faster than 7200 rpm, which means less than 0.55 of the τ parameter value.

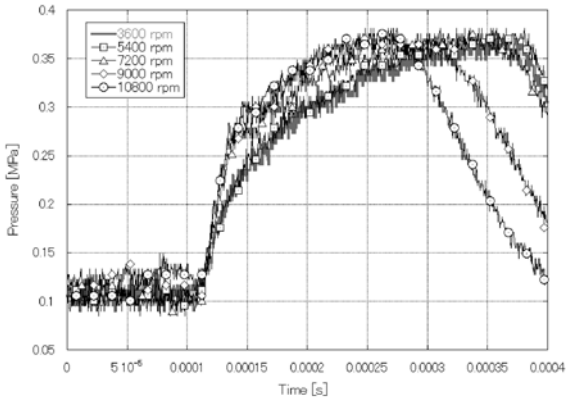

Fig.10 Pressure Time Traces at the Stagnation (L=42 mm)

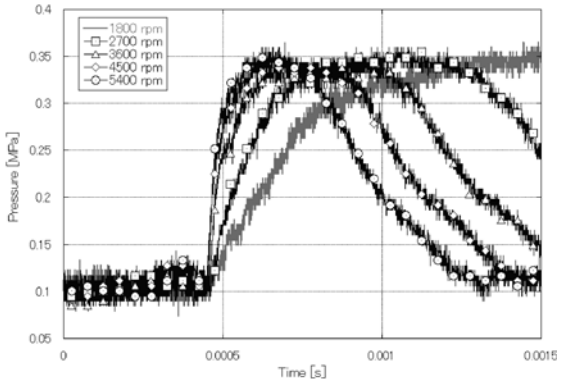

Fig.11 Pressure Time Traces at the Stagnation (L=168 mm)

Figure 11 shows the results of the longer test section. The similar trend is observed and the limiting rotor speed for shock wave generation seems to be 3600 rpm, which corresponds to 0.27 of τ parameter value. Here, it must be noticed that a shock wave can be generated even in this longer cell, if the rotor speed is fast enough. Furthermore, the rotor speed itself could be reduced from 7200 to 3600 rpm by extending the cell length with keeping the shock wave generation.

Comparison between Numerical and Experimental Results

Figure 12 shows a comparison of the results in pressure between numerical calculations and experimental measurements at the stagnation position in the shorter test section. Here, the numerical simulation was performed for Case 'S3' (L=42 mm, 7200 rpm). As seen in this figure, the numerical result shows excellent agreement with the experimental one. A little difference appears in the pressure increasing process just after the shock wave arrival. The reason of this difference is supposed that the pressure in the buffer tank oscillated by the ports' rotation in the experiment, while the upstream pressure was set as constant in the numerical simulation.

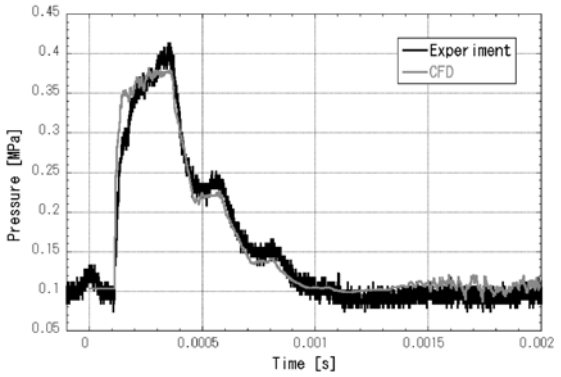

Fig.12 Comparison of Numerical and Experimental Results (Stagnation Pressure, L=42 mm)

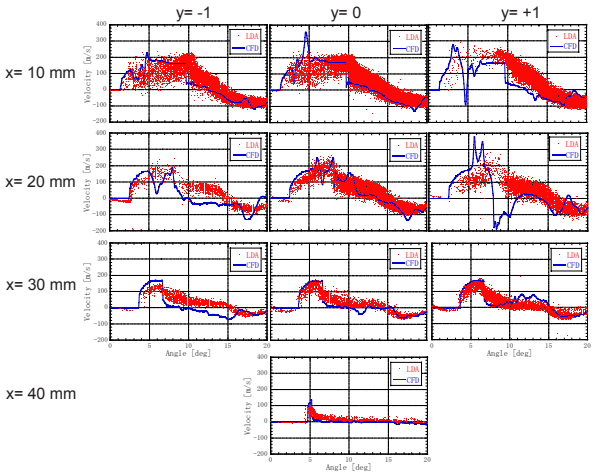

Fig.13 Comparison of Numerical and Experimental Results (Axial Velocity, L=42 mm)

On the other hand, the decreasing rate of the pressure shows good agreement, so that the estimation of the leakage is appropriate in the present simulation.

Figure 13 shows the comparison of the flow velocity at each measuring point of LDA. At the measuring points of x=10 mm, the maximum velocity at y=0 in the numerical result is extremely high compared to those at y=1 and –1, while it does not differ so much among these three measuring points in the experimental results. The reason of this extreme acceleration in the numerical result is that an aerodynamic throat is formed by two vortices near to the cell walls (Fig.14). This phenomenon is closely related to the flow structure at the contact surface between the driver and driven gases. However, the flow structure at the contact surface is much influenced by the leading edge of the cell wall, according to the previous numerical work[11]. Therefore, it is not appropriate to discuss this phenomenon with the present numerical results. The similar phenomenon also appears at the measuring point of (x, y)=(20, +1) mm.

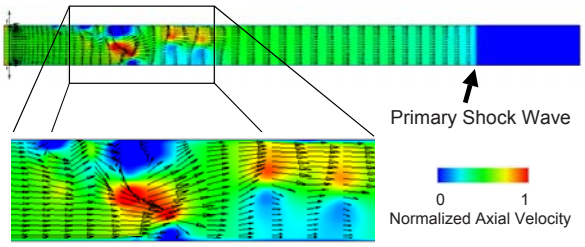

Fig.14 Aerodynamic Throat (Contour: axial velocity normalized by the sound speed, L=42mm, Rotor Angle: 4 degree)

Except for this discrepancy, the time traces of the flow velocity show good agreement. As a result, it was confirmed numerically and experimentally that the effect of wall boundary layer is not serious and the shock waves can propagate in this small cell.

Conclusion

In the present study, the internal flow dynamics in the small cells for micro wave rotors were carefully investigated in both numerical and experimental approaches. In the experiment, a new type of test equipment was used to visualize the internal flow dynamics with shock wave propagation in the small tubes of different lengths. In the schlieren pictures, the generation and propagation of shock waves were observed clearly in both cases without obvious interaction with the wall boundary layer. Also the flow velocity was measured by LDA, and it was revealed that the wall boundary layer thickness was less than 0.5 mm, which seems to be small enough for shock wave propagation. Furthermore, the measurement of stagnation pressure revealed that the shock wave was generated even in the longer cell if the rotor speed is fast enough. Also, it was confirmed that the rotor speed could be reduced with keeping the shock wave generation by adopting the longer cell in the present range of the design parameter values.

Acknowledgement

The present work was financially supported through the Grants-in-Aid for Scientific Research by the Ministry of Education, Culture, Sports, Science and Technology.

References

[1] Nagashima, T. et al., “Lessons learnt from Ultra-Micro Gas Turbine Development at University of Tokyo,” Invited Lecture, von Karman Institute for Fluid Dynamics Lecture Series on Micro Gas Turbines, Brussels, 2005

[2] Epstein, A.H., et al., “Micro-Heat Engines, Gas Turbines, and Rocket Engines,” AIAA Paper 97–1773, Jun. 1997

[3] Fatsis, A., and Ribaud, Y., “Thermodynamic analysis of gas turbines topped with wave rotors,” Aerospace Science and Technology, no. 5, 1999, pp. 293–299

[4] Snyder, P.H., and Fish, R.E., “Assessment of a Wave Rotor Topped Demonstrator Gas Turbine Engine Concept,” ASME Paper 96-GT-41, June 1996

[5] Larosiliere, L.M., “Wave Rotor Charging Process: Effects of Gradual Opening and Rotation,” Journal of Propulsion and Power, Vol. 11, No. 1, Jan.–Feb. 1995, pp. 178–184

[6] Araki, M., Arai, M., Okamoto, K., Ishima, T., and Obokata, T., “LDA Measurement of an Intermittent High-Speed Flow inside a Micro Wave Rotor Cell,” Proceedings of 2007 Fuels and Emissions Conference (CD-Rom), 2007, SAE Paper 2007-01-0010

[7] Chakravarthy, S.R., and Osher, S., “A New Class of High Accuracy TVD Schemes for Hyperbolic Conservation Laws,” AIAA Paper 85-0363, Jan. 1985

[8] Anderson, W.K., Thomas, J.L., and Van Leer, B., “A Comparison of Finite Volume Flux Vector Splitting for the Euler Equations,” AIAA Paper 85-0122, Jan. 1985

[9] Jameson, A., Schmidt, W., and Turkel, E., “Numerical Solutions of the Euler Equations by Finite Volume Methods Using Runge-Kutta Time-Stepping,” AIAA Paper 81–1259, Jun. 1981

[10] Toro, E.F., “Riemann Solvers and Numerical Methods for Fluid Dynamics,” Springer, 1997, ISBN3-540-61676-4

[11] Okamoto, K., and Nagashima, T., “Visualization of Wave Rotor Inner Flow Dynamics,” Journal of Propulsion and Power, Vol.23, No.2, March-April, pp. 292–300, 2007

[12] Paxson, D.E., “Comparison Between Numerically Modeled and Experimentally Measured Wave-Rotor Loss Mechanisms,” Journal of Propulsion and Power, Vol. 11, No.5, Sep.–Oct. 1995, pp. 908–914

[13] Wilson, J., “An Experimental Determination of Losses in a Three-Port Wave Rotor,” Journal of Engineering for Gas Turbine and Power, Vol. 120, 1998, pp. 833–842

[14] Gyarmathy, G., “How Does the Comprex® Pressure-Wave Supercharger Work?” SAE Technical Paper 830234, 1983